Assessment of Kinome-Wide Activity Remodeling upon Picornavirus Infection

Authors

Tim S. Veth, Lonneke V. Nouwen, Marleen Zwaagstra, Heyrhyoung Lyoo, Kathryn A. Wierenga, Bart Westendorp, Maarten A. F. M. Altelaar, Celia Berkers, Frank J. M. van Kuppeveld, and Albert J. R. Heck

Correspondence

a.j.r.heck@uu.nl

In Brief

When viruses invade host cells a complex battle unfolds between the host and the pathogen: the virus seeks replication while the host cell strives to survive. Viruses purposedly alter the activity of host kinases during this interaction. Here, proteome-wide kinase activity assays capture these changes quantitatively, offering a comprehensive view of kinase regulation during picornavirus infection. The assays revealed numerous key kinases to be involved. By employing kinase inhibitors, we validated the role of activated kinases.

Graphical Abstract

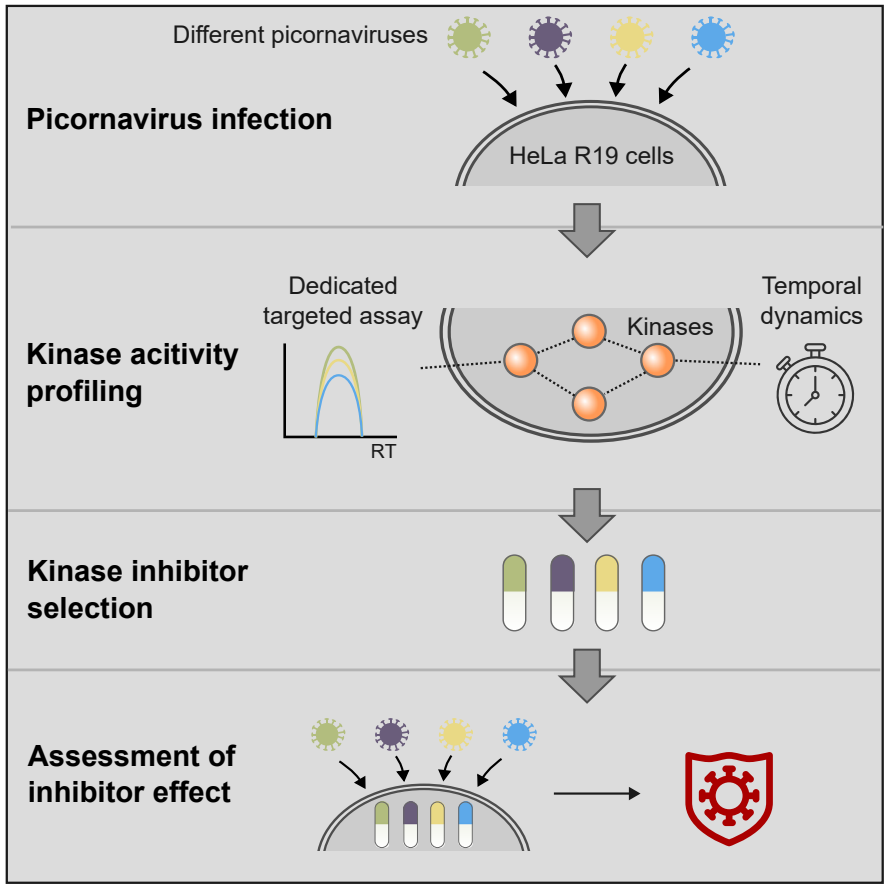

Highlights

- Targeted mass spectrometry quantifies kinome activity remodeling upon viral infection.
- Different picornaviral infections lead to shared and distinct kinome activity alterations.
- Viral security proteins are involved in kinome activity remodeling.
- Picornaviruses respond to kinase inhibitors, albeit with narrow therapeutic windows.

2024, Mol Cell Proteomics *23*(*5*), 100757

https://doi.org/10.1016/j.mcpro.2024.100757

Assessment of Kinome-Wide Activity Remodeling upon Picornavirus Infection

Tim S. Veth[1,2,‡], Lonneke V. Nouwen[3,‡], Marleen Zwaagstra[3], Heyrhyoung Lyoo[3], Kathryn A. Wierenga[4], Bart Westendorp[4], Maarten A. F. M. Altelaar[1,2], Celia Berkers[4], Frank J. M. van Kuppeveld[3,§], and Albert J. R. Heck[1,2,*,§]

Picornaviridae represent a large family of single-stranded positive RNA viruses of which different members can infect both humans and animals. These include the enteroviruses (*e.g.*, poliovirus, coxsackievirus, and rhinoviruses) as well as the cardioviruses (*e.g.*, encephalomyocarditis virus). Picornaviruses have evolved to interact with, use, and/or evade cellular host systems to create the optimal environment for replication and spreading. It is known that viruses modify kinase activity during infection, but a proteome-wide overview of the (de)regulation of cellular kinases during picornavirus infection is lacking. To study the kinase activity landscape during picornavirus infection, we here applied dedicated targeted mass spectrometry-based assays covering ~40% of the human kinome. Our data show that upon infection, kinases of the MAPK pathways become activated (*e.g.*, ERK1/2, RSK1/2, JNK1/2/3, and p38), while kinases involved in regulating the cell cycle (*e.g.*, CDK1/2, GWL, and DYRK3) become inactivated. Additionally, we observed the activation of CHK2, an important kinase involved in the DNA damage response. Using pharmacological kinase inhibitors, we demonstrate that several of these activated kinases are essential for the replication of encephalomyocarditis virus. Altogether, the data provide a quantitative understanding of the regulation of kinome activity induced by picornavirus infection, providing a resource important for developing novel antiviral therapeutic interventions.

Picornaviridae is a large family of small (~30 nm) non-enveloped viruses with a single-stranded positive-sense RNA genome (7.5–8 kb). This family currently comprises 68 documented genera, including the well-known *Enterovirus* and *Cardiovirus*. The enteroviruses consist of many important human pathogens such as poliovirus (causing paralytic poliomyelitis), coxsackieviruses, rhinoviruses (the cause of common colds, but also exacerbations of asthma and chronic obstructive pulmonary disease), as well as emerging viruses such as EV-D68 and EV-A71. The cardioviruses include important animal viruses such as encephalomyocarditis virus (EMCV) and Theiler's encephalomyelitis virus, but also the human pathogen Saffold virus (1). These viruses have severe impacts on human and animal health, but as of yet, vaccines are available only for poliovirus and for EV-A71 (in Southeast Asia), and no antiviral therapy is currently approved.

Picornaviruses contain a single open reading frame encoding a polyprotein that is autocatalytically cleaved by viral proteases into four structural proteins and seven or eight nonstructural proteins (2). The structural proteins form the viral capsid, whereas the nonstructural proteins are mainly involved in viral RNA replication and the modulation of host cell functions to create an environment wherein the virus can replicate efficiently. Although the sequence overlap between viruses of different genera is low, the replication strategy of these viruses is similar. Host cells are equipped with sensors and strategies to counteract viral infection. Upon viral infection, particularly viral replication, the host sensors can detect virus RNA, which elicits antiviral pathways such as the induction of stress responses leading to stress granules and interferon production and signaling. The activation of these pathways is disadvantageous for viral replication and production, and hence, viruses have evolved mechanisms to suppress these antiviral host responses. Within the picornavirus family, the leader proteins (*e.g.*, cardioviruses) and the 2A proteins (*e.g.*, enteroviruses) play key roles in suppressing stress and antiviral host responses and are therefore called the security proteins.

From the [1]Biomolecular Mass Spectrometry and Proteomics, Bijvoet Center for Biomolecular Research and Utrecht Institute for Pharmaceutical Sciences, Utrecht University, Utrecht, The Netherlands; [2]Netherlands Proteomics Center, Utrecht, The Netherlands; [3]Faculty of Veterinary Medicine, Virology Division, Department of Infectious Diseases and Immunology, Utrecht University, Utrecht, The Netherlands; [4]Faculty of Veterinary Medicine, Division of Cell Biology, Metabolism & Cancer, Department Biomolecular Health Sciences, Utrecht University, Utrecht, The Netherlands

[‡]These authors share first authorship.

[§]These authors share senior authorship.

*For correspondence: Albert J.R. Heck, a.j.r.heck@uu.nl.

https://doi.org/10.1016/j.mcpro.2024.100757

Although these proteins regulate similar processes, they are one of the least conserved proteins of the picornaviruses and execute their roles using distinct strategies (3, 4).

The human kinome is strongly involved in these essential host-virus interactions. The human kinome consists of over 500 kinases regulating cellular signaling by adding phosphate groups (phosphorylation) to proteins and other molecules (5). Each kinase can phosphorylate a limited repertoire of substrates, thereby regulating specialized cellular signaling (6, 7). Previously, we showed that upon infection with coxsackievirus B3 (CVB3), at least 85% of the phosphoproteome is dynamically regulated, substantiating the pertinent role of kinase activity during picornavirus infection (8). As a result of that study, we found mTORC1, a kinase complex involved in regulating many processes, to become inactivated during CVB3 infection. This inactivation led to an activation of transcription factor EB and, subsequently, the release of viruses *via* secretory autophagy. Other groups have also demonstrated that kinases are regulated during picornavirus infection, for example, the activation of extracellular signal-regulated kinase (ERK) or CaMK-II (9–15). However, a comprehensive overview of the (de)regulation of cellular kinases during picornavirus infection is still lacking.

Quantifying kinase activity remains challenging. Most kinases are low abundant, and their signaling pathways govern multiple kinases. Thus, a complete understanding of kinase activity entails system-wide and highly sensitive measurements (16, 17). Over the years, numerous impactful assays have been developed that increased the ability to probe kinase activity, such as heavy-labeled substrates-based assays (*e.g.*, KAYAK), probe-based assays (*e.g.*, Kinobeads and KiNativ), and substrate-coated microarrays (*e.g.*, PamChip) (18–23). These assays have extensively been used in research, leading to an increased understanding of kinase activity. Still, an assay that could reliably quantify kinase activity directly at the kinase level in a system-wide and highly sensitive manner was lacking. We have contributed to filling this gap by introducing targeted mass spectrometry assays that quantify the activity-determining phosphorylations in activation loops of kinases, providing a highly sensitive, multiplexed, system-wide kinase activity profile (24, 25).

Due to the low abundance and complex nature of kinase activation, prior efforts resulted in limited insights into a system-wide understanding of host-cell kinome activity remodeling by picornaviruses. To acquire such insights, we here aimed to quantify the regulated kinome dynamics upon virus infection, focusing on both CVB3 and EMCV in human HeLa R19 host cells, using our targeted mass spectrometry assays. Additionally, to probe specifically the role of the viral $2A^{pro}$ and L proteins, we also monitored the alterations in kinome activity induced by viruses harboring a CVB3-2A mutant containing a nonfunctional 2A protein (CVB3-$2A^{m}$) and an EMCV-L mutant containing a nonfunctional L protein (EMCV-L^{zn}). Altogether, the assay introduced here provides a unique system-wide view of the kinome activity remodeling taking place in host cells upon viral infection. Our findings contribute fundamental insights into viral infection and replication that may be used in the future development of new antiviral treatments to tackle picornavirus infections.

EXPERIMENTAL PROCEDURES

Cell Culture and Viral Infection

HeLa R19 and HEK293T cells were maintained in Dulbecco's modified Eagle's medium (Capricorn Scientific) supplemented with 10% fetal bovine serum and 1% Pen-Strep (Lonza). BHK-21 cells were cultured in Dulbecco's modified Eagle's medium containing sodium pyruvate and glutamax (Gibco; 2206106) and supplemented with 10% fetal bovine serum and 1% PEN-STREP (Lonza).

CVB3 and EMCV stocks were produced by passaging the virus on HeLa R19 cells. EMCV-L^{zn} was generated by producing RNA from the previously described pM16.1-VFETQG-Zn infectious clone, transfecting this RNA into BHK-21 cells, and passaging the virus once on BHK-21 cells (26, 27). CVB3-$2A^{m}$ was generated by introducing mutations in the catalytic site of 2A (H21A, D39A, and C110A) and a 3CD cleavage site between P1 and P2. RNA was produced from these infectious clones, transfected into HEK293T cells, and passed once in HEK293T cells. Renilla luciferase (Rluc)-CVB3 and nonsecretable Gaussia luciferase (Gluc)-EMCV were generated by producing RNA from their respective infectious clones (pRLuc-53CB3T7 for CVB3 and pdNGLuc-VFETQG-M16.1 for EMCV) and transfecting this RNA into HEK293T cells (28, 29). For all the viruses, the cultures were freeze-thawed three times, and cell debris was pelleted at 4,000*g* for 15 min upon the presence of complete cytopathic effect. Subsequently, the viral stocks were either aliquoted and stored at −80 °C directly or concentrated by ultracentrifugation (30% sucrose, 140,000*g* for 16 h, 4 °C, SW32Ti rotor), diluted in PBS, and stored at −80 °C. Virus titers were determined by endpoint titration on HeLa R19 and BHK-21 cells according to the Spearman–Kärber method and expressed as 50% tissue culture infectious dose (TCID50).

Cell Lysis, Protein Digestion, and Phosphopeptide Enrichment

HeLa R19 pellets were lysed, reduced, and alkylated in lysis buffer (1% sodium deoxycholate, 10 mM tris(2-carboxyethyl)phosphine hydrochloride), 40 mM chloroacetamide, and 100 mM TRIS, pH 8.0 supplemented with phosphatase inhibitor (PhosSTOP, Roche) and protease inhibitor (cOmplete mini EDTA-free, Roche). Cells were heated at 95 °C and sonicated with a probe sonicator to shear DNA. A bicinchoninic acid assay (Thermo Fisher Scientific) was used to determine the protein amount, after which samples were split into 200 μg aliquots. Proteins were digested overnight at 37 °C with trypsin (1:50 μg/μg) (Sigma-Aldrich) and lysyl endopeptidase (1:75 μg/μg) (Wako Chemicals), after which the heavy-labeled phosphorylated peptides were added to the samples. The sodium deoxycholate was precipitated twice with 2% formic acid, after which samples were desalted and enriched in an automated fashion using the AssayMap Bravo platform (Agilent Technologies) with corresponding AssayMap C18 reverse-phase column (Agilent Technologies) and Fe^{3+} tips for the enrichment of phosphorylated peptides (Agilent Technologies), as previously described (30).

Targeted Kinome Quantification of Virus-Infected Cells

The targeted kinome assay was adopted from assays described previously (24, 25). Heavy-labeled peptides are spiked-in and act as a reference for quantification of the endogenous peptides. Additionally, the assay utilizes optimized collision energies and retention

time-based peptide quantification to measure peptide fragments that reveal the phosphorylation site. Samples were analyzed on a TSQ Altis (Thermo Fisher Scientific) coupled to an UltiMate 3000 (Thermo Fisher Scientific) and an easy spray analytical column (ES802A, 25 cm, 75 mm ID PepMap RLSC, C18, 100 Å, 2 mm particle size column (Thermo Fisher Scientific)). Samples were loaded on a trap column (Acclaim PepMap 100 C18 HPLC Column 0.3 × 5 mm with 5 μm particles (Thermo Fisher Scientific)) with 2.2% Buffer A (0.1% formic acid) for 3 min, subsequently separated using 0 to 32% buffer B (99.9% acetonitrile, 0.1% formic acid) in 35 min at 300 nl/min, followed by a 20 min column wash with 80% buffer B at 300 nl/min, and 10-min column equilibration at 2.2% B. The TSQ Altis spray voltage was set at 1.9 kV and fragmented at 1.5 mTorr in the second quadrupole. The first quadrupole was set at 0.7 da full width at half maximum, and the third quadrupole was set at 1.2 da full width at half maximum. All transitions were measured with optimized collision energy within a 5-min window, and a cycle time of 5 s, resulting in more than 10 points across the peak.

Data Analysis of the Targeted Kinome Assay

All experiments were analyzed using Skyline-Daily (version 20.2.1.404) (https://skyline.ms/) (31). The quality of the peptides was assessed mainly on the signal correlations between the heavy and the light peptides. The most important aspects were perfect coelution, peak shape, and relative contributions of each transition between the heavy and the light peptide, and agreement with the expected retention time using indexed retention time (iRT) peptides. An rdotp >0.95 was maintained to indicate the similarity between the heavy and the light peptide. Further data visualization and analyses were done in R (version 4.1.3) (https://www.r-project.org/).

Effects of Kinase Inhibitors on CVB3 and EMCV Virus Production

To study the effect of the kinase inhibitors on CVB3 and EMCV virus production, infection was combined with endpoint titration. HeLa R19 cells (1*10^4 cells/well) were seeded in 96-well plates. The following day, the cells were infected with CVB3 or EMCV for 30 min (37 °C) at a multiplicity of infection of 5. Afterward, the inoculum was removed, and fresh (compound-containing) medium was added to the cells. After 7 h of infection, the plates for measuring total virus production were directly stored at −80 °C. After three freeze-thaw cycles, virus titers were determined by endpoint titration on HeLa R19 cells according to the method of Reed and Muench and expressed as 50% TCID50. For analysis of the titrations, GraphPad Prism (version 8) was used (https://www.graphpad.com/).

Effects of Kinase Inhibitors on CVB3 and EMCV RNA Replication

To study the effect of putative kinase inhibitors on CVB3 and EMCV replication, RLuc-CVB3 and GLuc-EMCV were used. Briefly, HeLa R19 cells (1*10^4 cells/well) were seeded in 96-well plates. The following day, the cells were infected with RLuc-CVB3 or GLuc-EMCV for 30 min (37 °C) at a multiplicity of infection of 0.1. Subsequently, the inoculum was removed, and fresh (compound-containing) medium was added to the cells. The cells were lysed with 50 μl lysis buffer (Promega) at the appropriate time points and stored at −20 °C for further use. To measure the luminescence of the cell lysates, a Renilla assay system (Promega) was used according to the manufacturer's protocol. Graphpad Prism (version 8) was used to analyze the luciferase assays.

Cell Viability

To measure the effect of the kinase inhibitors on cell viability, the CellTiter 96 AQueous One Solution Cell Proliferation Assay (Promega) was used. HeLa R19 cells were seeded in 96-well plates at a density of 1*10^4 cells/well. After incubation with the compound for the appropriate time, the CellTiter 96 AQueous One Solution Reagent was added (10 μl/50 μl medium). This mix was incubated for 0.5 to 1 h at 37 °C, after which the absorbance was measured with an Elisa Plate reader at 490 nm. Viability was determined as the percentage of viable cells compared to the control (cells incubated with dimethylsulfoxide only).

Immunoblotting

Samples were either taken from the cell pellet of the proteomics samples (before lysis) or created in an independent experiment. In the latter case, HeLa R19 cells were seeded in 6-well plates at a density of 4*10^6 cells/well. The next day, the cells were infected for 30 min, after which the medium was refreshed, and the cells were incubated for the indicated time points. The cells were lysed using TEN-lysis buffer (100 mM Tris pH 8.0, 1 mM EDTA, 50 mM NaCl, 1% NP40, and protease inhibitor mix (Roche)). Postnuclear lysates were obtained by centrifugation at 15,000*g* at 4 °C for 15 min. Protein concentrations were determined using a bicinchoninic acid assay (Thermo Fisher Scientific). Cell lysates were mixed with Laemmli buffer, and 20-30 μg was resolved using a 10% SDS-PAGE gel. The proteins were transferred using the Trans-blot turbo system according to the manufacturer's protocol (Bio-Rad). After transferring, the membrane was washed 2 to 3 times with Tris-buffered saline with 0.1% Tween-20 detergent (TBST) and blocked with TBST + 5% bovine serum albumin for phosphoproteins and TBST+5% milk for nonphosphorylated proteins for 1 h at room temperature. The primary antibody was diluted in blocking buffer and incubated overnight at 4 °C. The secondary antibody was diluted again in TBST + 5% milk and incubated for 60 min at room temperature. For Western blot the following antibodies were used: γH2AX (Cell Signaling Technology; #2577, 1:1000), tubulin (Sigma-Aldrich; T6557, 1:5000), Anti-rabbit horseradish peroxidase-linked Antibody (Cell Signaling Technology; #7074, 1:3000), Anti-mouse horseradish peroxidase-linked Antibody (Cell signaling Technology; #7076, 1:3000). Between and after the antibody incubations, the membrane was washed three times with TBST. Finally, the membrane was developed using enhanced chemiluminescence reagents.

Experiment Design and Statistical Rationale

All treated and untreated cellular groups used in this study entailed n = 3 biological replicates unless specified otherwise. Samples used for the kinome activity assays were enriched for phosphorylated peptides, and all samples were injected separately into the liquid chromatography with tandem mass spectrometry system. Each raw file was separately evaluated using Skyline (31). This number was sufficient to assess reproducibility and quantitatively compare the various conditions.

RESULTS

Targeted Mass Spectrometry Assay for Assessing Kinome-Wide Activation Upon Viral Infection

We hypothesized that CVB3 and EMCV infection could broadly affect the host kinome. Therefore, to monitor kinome-wide dynamics upon picornavirus infection, a targeted mass spectrometry assay was set up that quantifies activity-determining phosphorylations in the activation loop of kinases, providing reliable, highly sensitive, and direct measurements (Fig. 1*A*). The assay consists of stable-isotope standards of ~480 phosphorylated peptides spanning

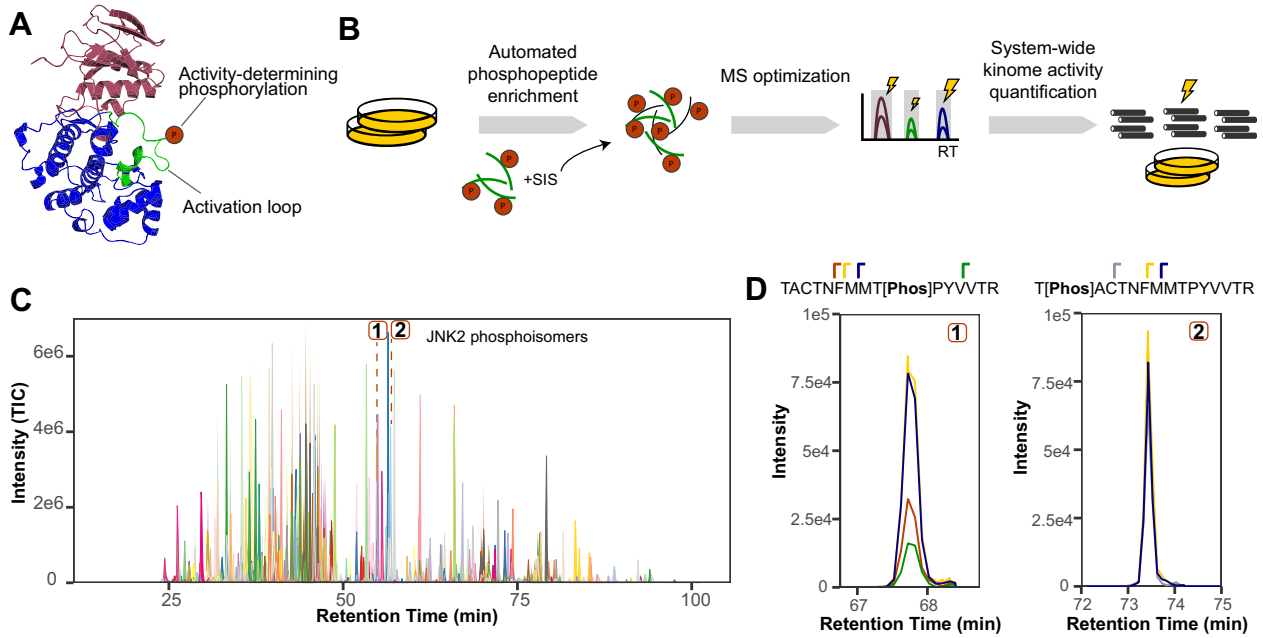

FIGURE 1. **Targeted mass spectrometry assay for assessing host-cellular kinome-wide activation upon viral infection.** *A*, most kinases share a universal domain structure, namely an N-lobe (*red*), a C-lobe (*blue*), and an activation loop (*green*). Kinase activity is determined by phosphorylation in the activation loop, providing a reliable proxy for kinase activity. *B*, experimental method overview. Phosphorylated stable isotope standards (SIS) corresponding to the endogenous activation loop peptides are added to the sample before automated desalting and phosphopeptide enrichment. Subsequently, the samples are measured using optimized mass spectrometry parameters, including transition-specific collision energies (CE) and retention time alignment using indexed retention time peptides (iRT peptides), resulting in an efficient and sensitive system-wide quantification of the kinome in a single LC-MS run. *C*, total ion chromatogram (TIC) from the activation loop peptides measured by the targeted kinome assay. Each of the 483 quantified kinase activation loops is represented by a different color, including the two JNK2 phosphoisomers (annotated). In these assays, nearly 100% of the measurement time is allocated to quantifying kinome activity. *D*, the extracted ion chromatograms (XIC) of the JNK2 phosphoisomers annotated in Figure 1*C*. The distinctive y-ions included in the targeted assay are represented using different colors. JNK, c-Jun N-terminal kinase.

nearly 200 kinases, covering about ~40% of the human kinome (Fig. 1*B*) (supplemental Table S1) (24, 25). Using this synthetic array of phosphopeptides, first fragmentation efficiencies were optimized by varying the collision energies of each transition (precursor ion and corresponding product ion after collision-induced dissociation fragmentation). Single-shot kinome activity measurements were facilitated by using iRT peptides and narrow isolation windows (32). As a result, nearly 100% of the measurement time is allocated to measuring kinase activation loop phosphorylation (Fig. 1*C*). Correct site localization is essential as possible phosphorylation sites (S/T/Y amino acids) are often in close proximity and may attribute to different biological functions (33, 34). In our assay, 420 of the 448 (~94%) phosphorylated activation loop peptides contain several putative phosphorylation sites, showing the necessity of correct phosphosite localization. While site localization for conventional bottom-up phosphoproteomic experiments is often challenging, our targeted assays use iRT peptides, an MS2 library, and phosphoisomer-specific product ions for unambiguous phosphosite localization (Fig. 1*D*) (35, 36). The ability to perform reliable single-shot measurements of system-wide kinase activity with confident site localization makes the here-used targeted kinome assay a prominent choice for quantifying kinome dynamics upon viral infection.

Highly Sensitive Quantification of Viral Kinome Regulation

To elucidate host-cell kinome activity remodeling upon infection, we infected HeLa R19 host cells with either CVB3 or EMCV. Subsequently, at different time points (4, 6, 8, and 10 hours post infection (h.p.i.)), the kinome assay was used to monitor in parallel 483 kinase activation loop phosphorylations.

CVB3 and EMCV belong to different genera within the family *Picornaviridea* (Fig. 2*A*), but use similar replication strategies. To investigate whether and how the security proteins $2A^{pro}$ (CVB3) and L (EMCV) potentially affect kinome activity remodeling, kinome dynamics were also quantified upon infection of HeLa R19 cells with either CVB3 harboring a nonfunctional 2A protein (CVB3-$2A^{m}$) or EMCV-L^{zn}.

The targeted assay provided quantifiable activity data for 69 host-cell kinases, of which 62 were significantly regulated in experiments with at least one out of the four tested viral infections (ANOVA, $p < 0.05$) (supplemental Table S2). This substantially lower number of detected kinases than that we

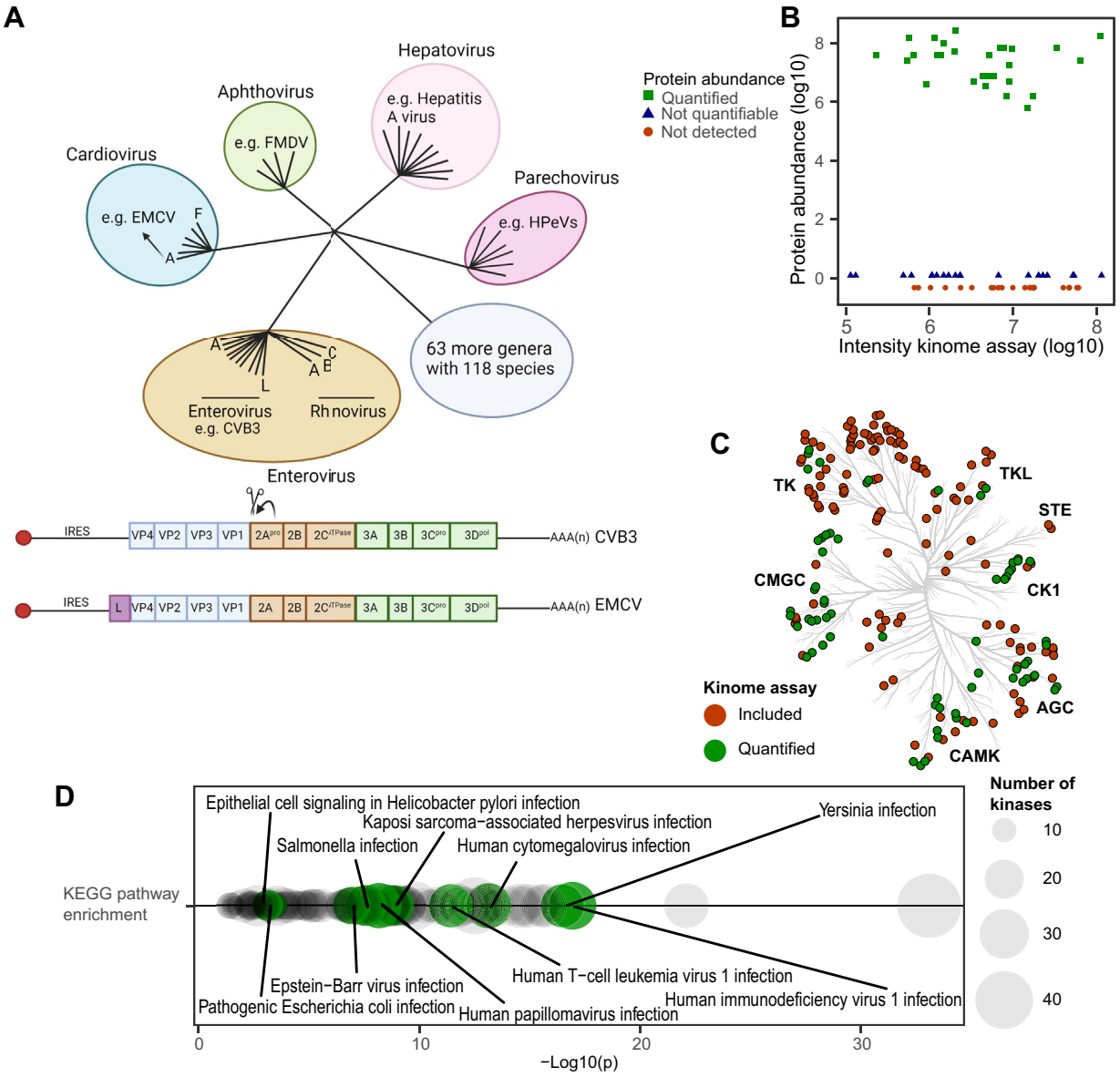

FIGURE 2. **System-wide kinome activity quantification clearly pinpoints toward viral infection.** *A*, phylogeny of the *picornaviridae* family. Although CVB3 and EMCV share an alike proteome organization, the sequences of their proteins exhibit marginal homology. *B*, kinase assay enables a deeper kinome depth. The kinase abundance (iBAQ values) quantified by Giansanti *et al*. (8) is plotted *versus* the signal intensity measured in the targeted kinome assay. Kinases quantified in both assays are displayed in *green*. The kinases quantified in the targeted kinome assay but below quantifiable limits in the proteomics data are shown in *blue*. Kinases only detected in the targeted kinome assay are displayed in *red*. *C*, kinome-tree representation of the kinases in the assay included (*red*) and detected (*green*) kinases. Kinases were determined as found when a phosphorylated peptide was reliably identified and quantified. *D*, KEGG enrichment analysis with kinases quantified in the targeted kinome assay (87) pinpoints broadly at various microbial, but mostly viral infections. CVB3, coxsackievirus B3; EMCV, encephalomyocarditis virus; iBAQ, intensity based absolute quantitation; KEGG, Kyoto Encyclopedia of Genes and Genomes.

targeted (*i.e.*, 69 out of ~200) is likely due to the absence or very low abundance of the "missed" kinases in the HeLa R19 cells. To validate if our kinome assay could quantify low abundant kinases, the detected signal in the targeted assay was compared to the kinase abundance quantified using bottom-up proteomics earlier reported by Giansanti *et al*. (8). Out of the 69 kinases, 28 (41%) were quantified both by the targeted assay and the proteomics measurements, 20 (29%) were quantified using the targeted assay but were below quantifiable limits in the proteomics measurements, and 21 (30%) were only detected in the targeted assay (Fig. 2*B*). The targeted assay enhances the depth in kinome profiling substantially by ~2.5 fold. This is further verified by the abundance of the identified kinases across the proteome, constituting the

full dynamic range of the proteome (supplemental Fig. S2). Altogether, the targeted kinome assay provides a sensitivity required for monitoring the activity of low abundant kinases putatively involved in picornavirus infection.

The targeted assay covered nearly all kinome families, representing kinases involved in diverse cellular processes (Fig. 2*C*). Interestingly, Kyoto Encyclopedia of Genes and Genomes pathway enrichment analysis of the quantified kinases revealed significant enrichments, notably for various viral infections, such as HIV and Kaposi sarcoma-associated herpesvirus infection (Fig. 2*D* and supplemental Table S3). ClueGO enrichment of the regulated kinases (independent triplicate measurements, ANOVA, $p < 0.05$) clusters 40% of the found gene ontology terms to the gene ontology term "Host-pathogen interaction of human Coronaviruses–mitogen-activated protein kinase (MAPK) signaling" (supplemental Fig. S3). These results provide confidence that the kinases we pick up as being regulated are relevant for microbial infections.

CVB3 and EMCV Infection Activates the MAPK Pathways and the DNA Damage Response

Next, we explore in detail the kinome activity remodeling upon either CVB3 or EMCV infection (Fig. 3*A*). Intriguingly, we observed, at first glance, very alike patterns of kinase activity remodeling, independent of which of the four viruses was used for infection. Of note, none of the here-found activated kinases showed an increase in abundance in the proteomics data of Giansanti (2020), suggesting that activation is primarily caused by the activation of inactive kinases instead of a change in kinase abundance. To organize the data, we used K-means clustering, which revealed 4 clusters that all show high similarity (Fig. 3*A*).

Two of these clusters represent host cell kinases that are highly activated, consisting primarily of kinases involved in MAPK signaling and the DDR (Fig. 3*A*). Activation loop phosphorylation increased up to 16 times with the maximum kinase activation between 6 and 10 h.p.i. The quantified MAPK signaling pathway consisted of MEK (MEK1 and MEK2) and ERK (ERK1 and ERK2), which are central activators of the MAPK pathway (37). Downstream of ERK or alternative MAPK pathways, the activation of stress-activated protein kinases was quantified, including c-Jun N-terminal kinases 1/2/3 (JNK1, JNK2, JNK3), and p38 (38). These stress-activated protein kinases are activated upon cellular stress, such as viral infections, and have been earlier reported to be induced by CVB3 and EMCV to facilitate viral infection (39–41). RSK1 and RSK2, downstream effectors of ERK that are involved in processes such as transcription and cell survival, were found to be increasingly activated upon infection (42–44).

CVB3 or EMCV infection also activated checkpoint kinase 2 (CHK2), a kinase known to become activated upon DNA damage (45, 46). Upon DNA double-stranded breaks, ataxia-telangiectasia mutated (ATM) and ataxia telangiectasia and Rad3 related (ATR) are activated. ATM and ATR subsequently activate CHK1 and CHK2, which activate several downstream effectors that together stall DNA replication and promote DNA repair. In our earlier work, based on the total phosphoproteome, we predicted that ATM and ATR were activated during infection (8).We now confirm the activation of the DDR by quantifying Ser-379 phosphorylation on CHK2 (with and without methionine oxidation) as a measure of CHK2 activation and found that both CVB3 and EMCV infection increased phosphorylation by 3 and 8 fold, respectively (Fig. 3*A*). This indicates that the DDR is activated during infection. CHK2 and the DDR have been reported to be regulated by various viruses (45–47), but the exact role of CHK2 and the DDR has remained unresolved. However, it is known that during rotavirus infection, CHK2 is activated and plays a role in viral replication even in the absence of DNA damage (48). To test whether there is DNA damage upon picornavirus infection, we performed a Western blot to quantify Ser-139 phosphorylation on histone H2AX (γH2AX), a well-accepted marker of DNA damage, and an ATM substrate, like CHK2 (Fig. 3, *B* and *C*) (49). In agreement with the observed kinase activation of CHK2, after 8 h, γH2AX abundance increased. This suggests that picornaviruses can induce DNA damage, and hence DDR is turned on. Altogether, our data suggest highly similar kinome activity remodeling upon CVB3 or EMCV infection, with the MAPK pathways and the DDR being at the center.

Both CVB3 and EMCV Infection Affect Kinases Involved in Cell Cycle Regulation

Besides kinase activation, our assay also reveals the deactivation of specific kinases. The cluster showing the most pronounced inactivation comprises cell cycle-regulating kinases, showing up to an 8-fold decrease in activity, some already becoming inactivated at 4 h.p.i. (Fig. 3*A*). Among these are several cyclin-dependent kinases (CDKs), namely CDK12, CDK1, and CDK2. CDKs are predominantly known for their role in the cell cycle (*e.g.*, CDK1 and CDK2), but several CDKs (*e.g.*, CDK12, CDK9, and CDK11) are key regulators of transcription that, for example, phosphorylate the C-terminal domain (CTD) of RNA polymerase II (Pol II) (50). The Greatwall kinase (GWL), a critical mitosis regulator, was also found to be deactivated.

Several other kinases became deactivated, many exhibiting broader functionality, such as HIPK3, the dual specificity tyrosine-phosphorylation-regulated kinase (DYRK) family of kinases, and the SRC family of kinases. Although these kinases execute diverse cellular processes, their main function has been attributed to the regulation of apoptosis, cell proliferation, and gene transcription (51–54). While the role of these kinases during infection is currently unknown,

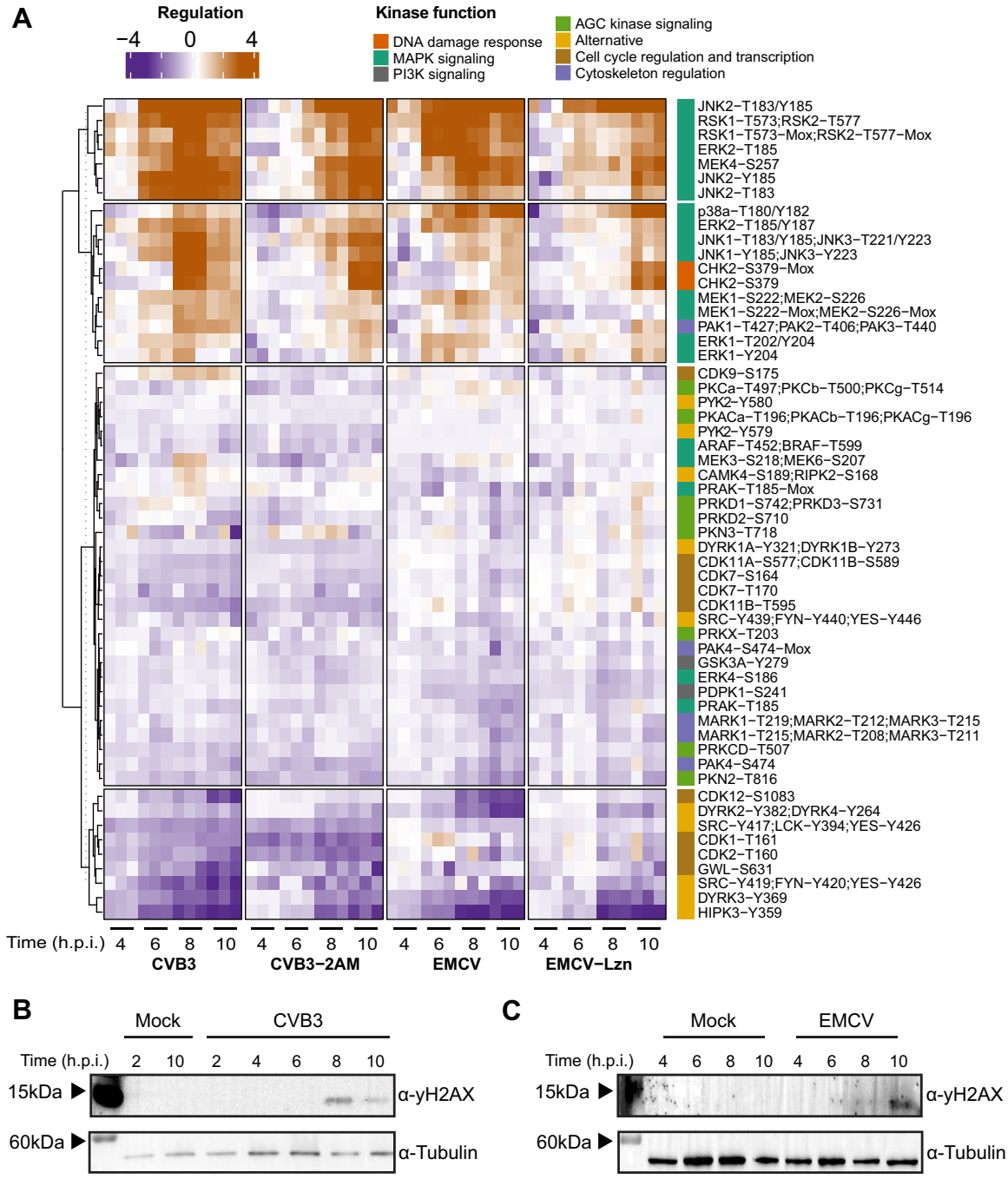

FIGURE 3. **Upon picornavirus infection by either CVB3 or EMCV, host cells display alike kinome activity remodeling.** *A*, upon infection of HeLa R19 host cells by either CVB3, EMCV, CVB3-2Am, or EMCV-L^{zn} (independent triplicate measurements, ANOVA, $p < 0.05$), highly alike regulation of system-wide kinome activation is observed. The reported values for activity-determining phosphorylation in the activation loop of the kinases represent the fold change (log2) compared to the 4 h.p.i. control (medium only). *Red* represents increased, and *blue* represents decreased kinase activity. Clustering was performed by using K-means clustering. Methionine oxidation is described as "Mox". *B* and *C*, Western blot analysis revealing the induction of γH2AX, an acknowledged marker of DNA damage (49) upon infection by CVB3 (*B*) or EMCV (*C*). As control, a mock was included, which was treated with culture medium. CVB3, coxsackievirus B3; EMCV, encephalomyocarditis virus; EMCV-L^{zn}, EMCV-L mutant containing a nonfunctional L protein.

DYRK2 and DYRK3 play a role in mitosis, and the SRC family of kinases is also implicated in cell cycle regulation (51, 53). Together with the inactivation of CDK1, CDK2, and GWL, this suggests that CVB3 and EMCV infection also modulates the cell cycle, although additional roles cannot be ruled out.

Subtle Differences in Kinome Activity Remodeling Induced by CVB3 or EMCV Infection

Although we observed high similarity in kinome activity remodeling upon CVB3 and EMCV infection, some differences were also detected. These can be subtle differences in dynamics or unique differences (kinases that are exclusively affected by either CVB3 or EMCV).

As previously described, the MAPK pathways and cell cycle kinases were regulated by CVB3 and EMCV, but there are subtle differences in the dynamics of this regulation (supplemental Fig. S4*A*). For example, a comparison of activation of p38 and RSK1/2 relative to MEKK4 (which is activated with similar dynamics by CVB3 and EMCV) shows that p38 activation is more profound upon EMCV infection and that maximal activation of RSK1/2 is reached earlier in EMCV-infected cells than in CVB3-infected cells. Notably, it was recently reported that the EMCV leader protein directly targets RSK1/2, leading to RSK1/2 activation (which will be further discussed in the next section) (42). Another difference is the inactivation of CDK1 and CDK2, both of which are much more strongly inhibited in cells infected with CVB3 than with EMCV (supplemental Fig. S4*B*).

There are also kinases that are exclusively affected by CVB3 or EMCV. CVB3 infection uniquely affects CDKs (CDK9, CDK11A, and CDK11B) and p21 activated kinases (PAK) (PAK1, PAK2, and PAK3), while EMCV uniquely regulated PYK2 (50% increase on Tyr-580 phosphorylation, Fig. 4*A*), a kinase whose role in picornavirus infection is unknown. The PAK kinases are involved in cytoskeleton regulation and in the entry of echovirus1 (an *Enterovirus*) through the activation of macropinocytosis (55). To test whether the PAK kinases have a role in CVB3 replication, we inhibited these kinases with FRAX597, but no decrease in viral replication was observed (supplemental Fig. S5).

The CDKs that we found to be differentially rewired all regulate the coordination of transcription and RNA processing, which are important processes during picornavirus infection (50, 56, 57). CDK9 was activated by CVB3 infection, but not by EMCV, whereas CDK11A and CDK11B were inactivated by CVB3, but not by EMCV infection. Regulation of CDKs during CVB3 infection has been described, however, the possible roles of CDK9, CDK11A, and CDK11B in these processes are unknown (58).

The Role of Viral Security Proteins

We also investigated the role of security proteins in kinome activity remodeling by infecting host cells with recombinant viruses that had either a nonfunctional protein 2A (CVB3-2A^{m}) or a nonfunctional protein L (EMCV-L^{zn}). Infection with these recombinant viruses resulted in a general delay in kinome activation of nearly all kinases, likely due to the delay in their replication. Notably, EMCV-L^{zn} infection showed decreased capabilities to activate MEK, ERK, and RSK relative to WT EMCV (Fig. 4*B*). Unlike CVB3-2A^{m}, EMCV-L^{zn} did not only show a delayed response, but the amplitude of activation did not reach the same level as for WT EMCV, hinting at a specific function of L in increasing RSK pathway activation (notably, 8 different quantified phosphorylation sites gave substantial confidence in differential RSK pathway activation). This agrees with the recent finding that cardiovirus L binds RSK, prevents its dephosphorylation and reroutes it to nucleoporins to trigger their hyperphosphorylation (42). Related, it has been described that L triggers hyperphosphorylation of nucleoporins by activating p38 and ERK (43). Together, our data suggest that RSK, ERK, and p38 signaling pathways are regulated by EMCV-L.

We hypothesize CVB3-2A^{m} and EMCV-L^{zn} also showed differential regulation of CDKs compared to the WT viruses. Only WT CVB3, but not CVB3-2A^{m}, activates CDK9, pointing to a role of 2A^{pro} in activating this kinase. Interestingly, the only CDK involved in transcription that is inactivated by both CVB3 and EMCV (CDK12) is not inactivated by either CVB3-2A^{m} or EMCV-L^{zn}, suggesting a role of 2A^{pro} and L in inhibiting this kinase (direct or indirect) and in regulating transcription (Fig. 4*C*).

Finally, we observed that both CVB3-2A^{m} and EMCV-L^{zn} still activated CHK2. However, whereas CVB3-2A^{m} and WT CVB3 activate CHK2 to a similar extent (both show a 5-fold increase in activity determining phosphorylation on CHK2 (Fig. 4*B*)), EMCV-L^{zn} infection did not result in a delay in CHK2 phosphorylation and even resulted in a 2-fold higher CHK2 phosphorylation than WT EMCV. This finding hints at the role of L in limiting CHK2 activation.

Role of MAPK Pathway and DDR Activation in the Viral Life Cycle

The observed activation of several kinases upon CVB3 or EMCV infection suggests a role of these kinases in viral reproduction. Therefore, we hypothesized that inhibition of these kinases may potentially decrease viral reproduction. To investigate this, we selected 16 available kinase inhibitors targeting these kinases. The inhibitors included MAPK pathway inhibitors, DDR inhibitors, an inhibitor of CDK9, and a pan-PAK kinase inhibitor (supplemental Table S4). To investigate the inhibitor effect on viral reproduction, each inhibitor was evaluated on luciferase-expressing viruses to monitor viral RNA replication and a TCID50 assay to determine viral titers at 7 h.p.i., which represents a single-round infection cycle (supplemental Table S5).

Nearly all 16 inhibitors could decrease viral reproduction (in minimally one assay), albeit most of them often only at relatively high concentrations (supplemental Table S5, Fig. 5, *A* and *B* and supplemental Fig. S5). However, almost all inhibitors also reduced cell viability at these higher concentrations, illustrating a likely narrow therapeutic window balancing effective treatment and cellular toxicity. Only a few inhibitors reduced viral RNA replication (luciferase assay, Fig. 5*A*) and virus production (TCID50 assay, Fig. 5*B*) at low concentrations

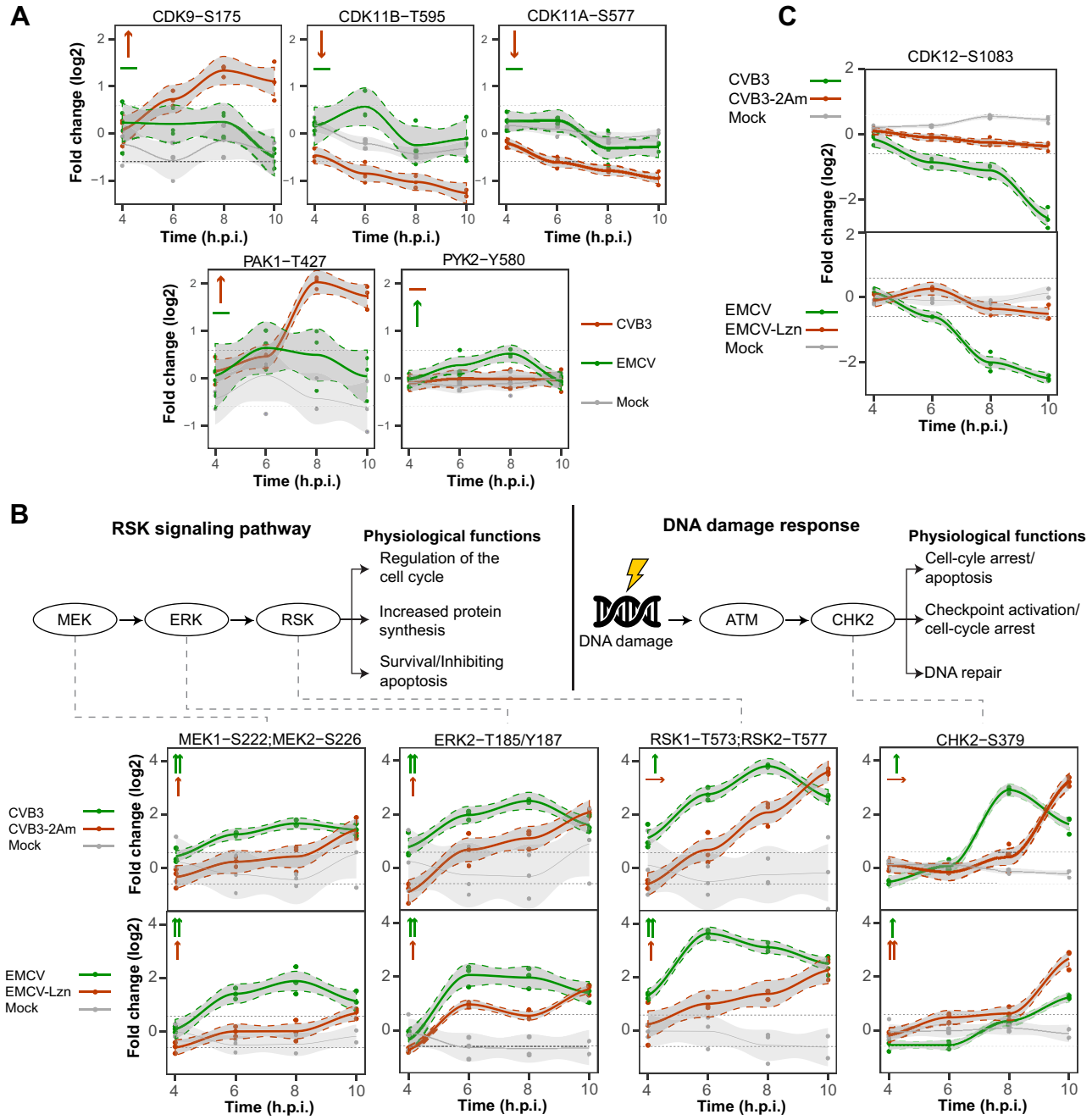

FIGURE 4. **Infection by CVB3-2A^{m} and EMCV-L^{zn} reveal both alike and distinct roles of 2A and L.** *A*, next to high similarity, WT CVB3 and WT EMCV induce a few additional unique kinase activations, as illustrated by *line plots* extracted from the targeted kinome assay. The *arrows* represent a positive or negative fold change, and a *line* represents no change in abundance. The gray areas represent the 90% confidence interval (independent triplicate measurements). *Dashed lines* represent a 50% increase or decrease in the activity determining phosphorylated peptides. The CDK11A-S577 peptide cannot be distinguished from the CDK11B-S589 peptide. The PAK1 peptide corresponds also to the same peptide of PAK2-T406 and PAK3-T440. *B*, *line plots* representing quantification of activity determining phosphorylation (log2 fold change compared to the 4 h.p.i. medium only control) of kinases in the RSK signaling pathway and the CHK2 regulated DNA damage response. Figure annotation is as in panel *A*. Additionally, the *upward arrow* signifies a rise in abundance, and two *upward arrows* indicate a larger increase. A *right-pointing arrow* depicts a delay in regulation. *C*, CDK12 line plots with similar annotation as in panel *A*. CDK, cyclin-dependent kinases; CVB3, coxsackievirus B3; EMCV, encephalomyocarditis virus; EMCV-L^{zn}, EMCV-L mutant containing a nonfunctional L protein; h.p.i, hours post infection; PAK, p21 activated kinase.

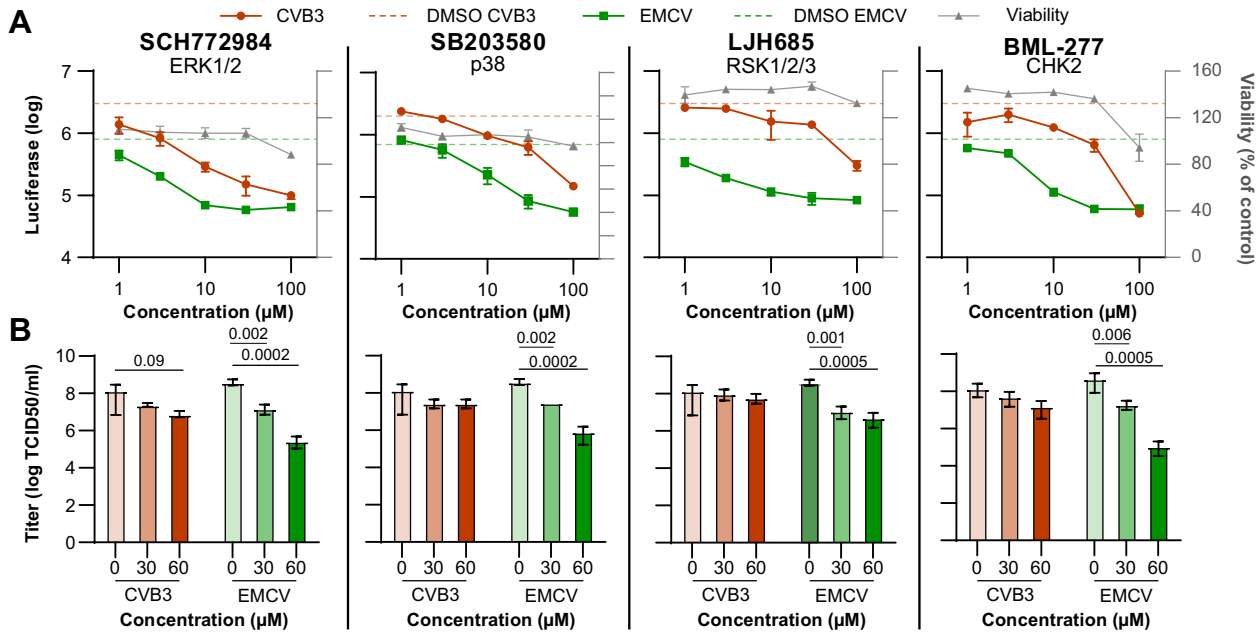

FIGURE 5. **Effect of kinase inhibitors on CVB3 or EMCV infection.** *A*, viral RNA replication was measured at 7 h.p.i. by measuring luciferase levels produced by luciferase-expressing viruses in cells treated with selected kinase inhibitors (independent triplicate measurements). CVB3-infected HeLa cells are represented in *orange*, EMCV-infected cells in *green*, and cell viability in *gray*. A DMSO-treated control was included, for which the luciferase readout is displayed by the *orange* and *green dotted lines*, representing CVB3 and EMCV, respectively. The whiskers depict the standard deviation. *B*, cells were infected with WT CVB3 or EMCV, treated with different concentrations of kinase inhibitors, incubated for 7 h, after which viral titers were determined by endpoint titrations and expressed in tissue culture infectious dose (TCID50). For the various inhibitors, significant reductions in CVB3 and EMCV titers were observed when compared to the DMSO control (independent triplicate measurements, two-sided *t* test). The whiskers depict the standard deviation. CVB3, coxsackievirus B3; DMSO, dimethylsulfoxide; EMCV, encephalomyocarditis virus; h.p.i, hours post infection.

when still no or just a minimal decrease in cell viability was observed, including LJH-685, SCH772984, SB203580, and BML-277, which inhibit RSK, ERK, p38, and CHK2, respectively. Notably, EMCV was observed to be more sensitive to inhibition by these compounds than CVB3, especially when inhibiting RSK and CHK2, suggesting that EMCV might be more reliant on these kinases than CVB3.

DISCUSSION

Picornavirus infections can cause a plethora of diseases in humans and animals and consequently have a large socio-economic impact (1). These viruses are known to deregulate key host-cellular processes, such as gene expression, nucleocytoplasmic trafficking, intracellular membrane organization, and transport, and stress responses of the cell (59–62). It is known that picornaviruses remodel the activation of specific kinases (8–10, 12, 15, 63, 64), but a comprehensive overview of the (de)regulation of cellular kinases during picornavirus infection was lacking. Here, we aimed to provide a detailed map of the activity remodeling of the host cell kinome upon picornavirus infection using a targeted mass spectrometry-based system-wide kinase activation assay. In our assay, we included CVB3, EMCV, and two mutant viruses harboring either a nonfunctional $2A^{pro}$ protein (CVB3-$2A^{pro}$) or L protein (EMCV-L^{zn}). These nonstructural proteins belong to the so-called security proteins of picornaviruses that are pivotal in combating antiviral responses elicited by the host.

We observed a considerable overlap in the kinome activity remodeling of the host cells infected by either CVB3 or EMCV. The MAPK pathways and the DDR become activated, although the dynamics of activation of specific kinases within these pathways were different for CVB3 or EMCV. For example, RSK1/2 reached the maximal activation earlier for EMCV compared to CVB3, and p38 was activated stronger upon EMCV compared to CVB3 infection. It has been reported that the EMCV L protein can bind to RSK and inhibit the removal of the activity-determining phosphorylation by phosphatases, resulting in a constitutively activated RSK that is targeted by L to hyperphosphorylated nucleoporins leading to a nucleocytoplasmic trafficking disorder (NCTD) (42, 65). Consistent with these findings, we observed high and sustained RSK activation in EMCV-infected cells but only marginal RSK activation during infection with EMCV-L^{zn}. Our data also revealed that EMCV-L^{zn} infection decreased MEK and ERK activation, which activate RSK, implying that L inhibits RSK dephosphorylation and increases RSK phosphorylation through MEK-ERK activation. These findings agree with earlier reports that inhibition of ERK and p38 prevented L-induced NCTD (43). Consistently, we observed that EMCV replication

was sensitive to RSK, ERK, and p38 inhibition. Considering the binding of L to RSK, the activation of p38 and ERK, and the differences in the dynamics in MEK, ERK, and RSK activation that we observe upon EMCV-L^{zn} infection, we hypothesize that L-triggered activation of kinases upstream of RSK and the L-mediated inhibition of dephosphorylation of RSK together regulate the function of L.

Although we did not observe a pronounced effect of inhibitors of RSK, MEK, and ERK on CVB3 replication, activation of these pathways may play a role in regulating virus release, cytokine secretion, cell death, and/or another process during CVB3 infection, which might be relevant or the outcome of infection *in vivo*. For instance, it has already been described that the inhibition of p38 has a role in CVB3 release and that apoptosis might be regulated through the activation of MAPK pathways (66–68).

Infection by CVB3 or EMCV also activated CHK2, a kinase that is part of the DDR. The induction of yH2Ax, a marker of DNA damage further confirmed activation of the DDR. Activation of DDR upon CVB3 infection is in agreement with our earlier phosphoproteomics study, which already hinted at the activation of several kinases involved in the DDR, such as ATM, ATR, CHK1, CHK2, and aurora kinases (8). Also, for other enteroviruses, in particular EV-D68 and EV-A71, activation of the DDR and the presence of DNA damage has been reported (15, 69), suggesting that induction of DNA damage is a common phenomenon among picornavirus infection. Also, for other viruses (*e.g.*, HIV, human papillomavirus, rotavirus, and influenza A virus), activation of the DDR and the presence of DNA damage has been reported, which is often linked to reactive oxygen species production, DNA replication, and cell cycle inhibition (46, 70–75). However, especially for RNA viruses, the exact causes and consequences of the activation of the DDR are yet to be understood. In our experiments, inhibition of CHK2 did not affect CVB3 replication, yet reduced EMCV replication. Obviously, similar to that described above, activation of the DDR pathway by CVB3 may be important for alternative, postreplication steps and, thereby, in the outcome of infection *in vivo*. How inhibition of the DDR reduces EMCV replication remains to be established. Strikingly, CHK2 was activated more strongly by EMCV-L^{zn} than EMCV WT. Further studies into the regulation of the DDR in picornavirus-infected cells are needed to unravel more about the underlying mechanisms.

During both CVB3 and EMCV infection, several kinases involved in regulating the cell cycle became affected (*e.g.*, cyclin-dependent kinase (CDK)1/2 and the GWL). Interestingly, most of these have roles within mitosis, suggesting that both viruses regulate cell cycle, especially mitosis. Deregulation of the cell cycle has been observed before upon CVB3 and EMCV infection (76–78). Also, for EV-D68 and EV-A71, cell cycle deregulation has been observed (79, 80). However, in all these cases, different mechanisms can underlie the interference of the cell cycle. For instance, it has been described that one of the structural proteins of CVB3, VP1, can interact with CDK complexes, thereby inhibiting proliferation, but also that cyclin D is degraded upon CVB3 infection. Moreover, DNA damage can also be a trigger to halt the cell cycle (58, 77). All in all, we observe an inhibition of kinases that regulate the cell cycle, but further studies are needed to reveal the exact mechanisms.

Notably, apart from CDKs involved in the cell cycle, also transcriptional CDKs are affected upon infection. Transcriptional CDKs are kinases involved in transcriptional control and associated processes such as RNA capping, splicing, and chromatin remodeling. Among these transcriptional CDKs are CDK7, CDK8, CDK9, CDK11, and CDK12 (50). CDK12, known to phosphorylate the CTD of polymerase II and to regulate the expression of genes involved in DNA repair, was affected by both CVB3 or EMCV but not by the mutant viruses (81, 82). CDK11, implicated in regulating transcription and cell cycle progression, was inhibited by CVB3, while CDK9, also involved in phosphorylating the CTD of polymerase II, was activated by CVB3 but not by CVB3-$2A^{m}$ nor by EMCV or EMCV-L^{zn} (83, 84). For both CVB3 and EMCV, it is known that cellular transcription is rapidly inhibited after infection. The 3C protease and/or its precursors can enter the nucleus probably *via* a combination of a nucleus localization signal and the induction of NCTD (62, 85, 86). It has been reported that 3CD can cleave several transcription factors in the nucleus during enterovirus infection, thereby inhibiting cellular transcription (62). For CDK12 and CDK9, we observed a differential activation between the WT and the mutant viruses. Notably, no such differential regulation was observed for the other CDKs. Since the induction of NCTD is severely impaired during the infection with the mutant viruses, it is possible that the absence of the NCTD and, therefore, a hampered translocation of 3C to the nucleus and inhibition of cellular transcription leads to differential regulation of transcriptional CDKs. Together, our findings indicate that both CVB3 and EMCV regulate transcription, although likely through different mechanisms, and that the security proteins might be involved in this regulation.

Altogether, this research contributes to understanding system-wide kinome regulation upon picornavirus infection by providing a quantitative overview of kinome activity dynamics. We demonstrate that both CVB3 and EMCV activate MAPK pathways and the DDR while inhibiting kinases involved in cell cycle regulation and that EMCV replication is sensitive to inhibition of the activated kinases. Our data increase insights into picornavirus-induced infections with the potential to contribute to new therapeutics.

DATA AVAILABILITY

Targeted raw data files and all Skyline documents have been deposited in the ProteomeXChange Consortium

(identifier PXD046598) *via* Panorama Public (https://panoramaweb.org/xPLtbS.url).

All R scripts and corresponding input files can be downloaded from https://github.com/TVeth/Viral_kinome_Veth_2024

Supplemental data—This article contains supplemental data.

Acknowledgments—This work has been supported by the NWO funded Netherlands Proteomics Centre through the National Road Map for Large-scale Infrastructures program X-Omics, Project 184.034.019, and by CARE, a project that has received funding from the Innovative Medicines Initiative 2 Joint Undertaking (JU) under grant agreement No 101005077.

Author contributions—T. S. V., L. V. N., M. Z., H. L., K. A. W., B. W., M. A. F. M. A., C. B., F. J. M. K., and A. J. R. H. investigation; T. S. V., L. V. N., M. A. F. M. A., F. J. M. K., and A. J. R. H. conceptualization; T. S. V., L. V. N., M. A. F. M. A., C. B., M. A. F. M. A., F. J. M. K., and A. J. R. H. methodology; T. S.V., M. A. F. M. A., F. J. M. K., and A. J. R. H. data curation; T. S. V., L. V. N., M. A. F. M. A., C. B., F. J. M. K., and A. J. R. H. writing–review and editing; T. S.V., L. V. N., and A. J. R. H. writing–original draft; T. S.V. and L. V. N., formal analysis; T. S.V. and L. V. N., visualization; T. S.V. validation; M. A. F. M. A., C. B., F. J. M. K., and A. J. R. H. resources; M. A. F. M. A., C. B., F. J. M. K., and A. J. R. H. supervision; C. B., F. J. M. K., and A. J. R. H. funding acquisition; F. J. M. K. and A. J. R. H. project administration.

Conflict of interest—The authors declare no competing interests.

Abbreviations—The abbreviations used are: ATM, ataxia-telangiectasia mutated; CDK, cyclin-dependent kinases; CHK, checkpoint kinase; CTD, C-terminal domain; CVB3, coxsackievirus B3; DDR, DNA damage response; DYRK, dual specificity tyrosine-phosphorylation-regulated kinase; EMCV, encephalomyocarditis virus; EMCV-L^{zn}, EMCV-L mutant containing a nonfunctional L protein; ERK, extracellular-signal-regulated kinase; GWL, Greatwall kinase; h.p.i, hours post infection; iRT, indexed retention time; JNK, c-Jun N-terminal kinase; MAPK, mitogen-activated protein kinase; NCTD, nucleocytoplasmic trafficking disorder; TBST, Tris-buffered saline with 0.1% Tween-20 detergent; TCID50, tissue culture infectious dose.

Received December 17, 2023, and in revised form, March 16, 2024
Published, MCPRO Papers in Press, March 30, 2024, https://doi.org/10.1016/j.mcpro.2024.100757

REFERENCES

1. Whitton, J. L., Cornell, C. T., and Feuer, R. (2005) Host and virus determinants of picornavirus pathogenesis and tropism. *Nat. Rev. Microbiol.* **3**, 765–776
2. Baggen, J., Thibaut, H. J., Strating, J. R. P. M., and van Kuppeveld, F. J. M. (2018) The life cycle of non-polio enteroviruses and how to target it. *Nat. Rev. Microbiol.* **16**, 368–381
3. Agol, V. I., and Gmyl, A. P. (2010) Viral security proteins: counteracting host defences. *Nat. Rev. Microbiol.* **8**, 867–878
4. Porter, F. W., and Palmenberg, A. C. (2009) Leader-induced phosphorylation of nucleoporins correlates with nuclear trafficking inhibition by cardioviruses. *J. Virol.* **83**, 1941–1951
5. Manning, G., Whyte, D. B., Martinez, R., Hunter, T., and Sudarsanam, S. (2002) The protein kinase complement of the human genome. *Science* **298**, 1912–1934
6. Brinkworth, R. I., Breinl, R. A., and Kobe, B. (2003) Structural basis and prediction of substrate specificity in protein serine/threonine kinases. *Proc. Natl. Acad. Sci. U. S. A.* **100**, 74–79
7. Miller, C. J., and Turk, B. E. (2018) Homing in: mechanisms of substrate targeting by protein kinases. *Trends Biochem. Sci.* **43**, 380–394
8. Giansanti, P., Strating, J. R. P. M., Defourny, K. A. Y., Cesonyte, I., Bottino, A. M. S., Post, H., *et al*. (2020) Dynamic remodelling of the human host cell proteome and phosphoproteome upon enterovirus infection. *Nat. Commun.* **11**, 4332
9. Basta, H. A., Bacot-Davis, V. R., Ciomperlik, J. J., and Palmenberg, A. C. (2014) Encephalomyocarditis virus leader is phosphorylated by CK2 and Syk as a requirement for subsequent phosphorylation of cellular nucleoporins. *J. Virol.* **88**, 2219–2226
10. Guedán, A., Swieboda, D., Charles, M., Toussaint, M., Johnston, S. L., Asfor, A., *et al*. (2017) Investigation of the role of protein kinase D in human rhinovirus replication. *J. Virol.* **91**, e00217-17
11. Lim, B.-K., Nam, J.-H., Gil, C.-O., Yun, S.-H., Choi, J.-H., Kim, D.-K., *et al*. (2005) Coxsackievirus B3 replication is related to activation of the late extracellular signal-regulated kinase (ERK) signal. *Virus Res.* **113**, 153–157
12. Lin, D., Dong, X., Xiao, X., Xiang, Z., Lei, X., and Wang, J. (2023) Proteomic and phosphoproteomic analysis of responses to enterovirus A71 infection reveals novel targets for antiviral and viral replication. *Antivir. Res.* **220**, 105761
13. Nie, J., Ta, N., Liu, L., Shi, G., Kang, T., and Zheng, Z. (2020) Activation of CaMKII via ER-stress mediates coxsackievirus B3-induced cardiomyocyte apoptosis. *Cell Biol. Int.* **44**, 488–498
14. Shi, W., Hou, X., Peng, H., Zhang, L., Li, Y., Gu, Z., *et al*. (2014) MEK/ERK signaling pathway is required for enterovirus 71 replication in immature dendritic cells. *Virol. J.* **11**, 227
15. Zhao, Y., Li, L., Wang, X., He, S., Shi, W., and Chen, S. (2022) Temporal proteomic and phosphoproteomic analysis of EV-A71-infected human cells. *J. Proteome Res.* **21**, 2367–2384
16. Berginski, M. E., Moret, N., Liu, C., Goldfarb, D., Sorger, P. K., and Gomez, S. M. (2021) The Dark Kinase Knowledgebase: an online compendium of knowledge and experimental results of understudied kinases. *Nucleic Acids Res.* **49**, D529–D535
17. Casado, P., Rodriguez-Prados, J.-C., Cosulich, S. C., Guichard, S., Vanhaesebroeck, B., Joel, S., *et al*. (2013) Kinase-substrate enrichment analysis provides insights into the heterogeneity of signaling pathway activation in leukemia cells. *Sci. Signal.* **6**, rs6
18. Adams, J. A. (2003) Activation loop phosphorylation and catalysis in protein kinases: is there functional evidence for the autoinhibitor model? *Biochemistry* **42**, 601–607
19. Bantscheff, M., Eberhard, D., Abraham, Y., Bastuck, S., Boesche, M., Hobson, S., *et al*. (2007) Quantitative chemical proteomics reveals mechanisms of action of clinical ABL kinase inhibitors. *Nat. Biotechnol.* **25**, 1035–1044
20. Kubota, K., Anjum, R., Yu, Y., Kunz, R. C., Andersen, J. N., Kraus, M., *et al*. (2009) Sensitive multiplexed analysis of kinase activities and activity-based kinase identification. *Nat. Biotechnol.* **27**, 933–940
21. Patricelli, M. P., Nomanbhoy, T. K., Wu, J., Brown, H., Zhou, D., Zhang, J., *et al*. (2011) *In situ* kinase profiling reveals functionally relevant properties of native kinases. *Chem. Biol.* **18**, 699–710
22. Peterson, R. T., and Schreiber, S. L. (1999) Kinase phosphorylation: keeping it all in the family. *Curr. Biol.* **9**, R521–R524
23. Schutkowski, M., Reimer, U., Panse, S., Dong, L., Lizcano, J. M., Alessi, D. R., *et al*. (2004) High-content peptide microarrays for deciphering kinase specificity and biology. *Angew. Chem. Int. Ed.* **43**, 2671–2674

24. Schmidlin, T., Debets, D. O., van Gelder, C. A. G. H., Stecker, K. E., Rontogianni, S., van den Eshof, B. L., *et al*. (2019) High-throughput assessment of kinome-wide activation states. *Cell Syst.* **9**, 366–374.e5
25. Veth, T. S., Francavilla, C., Heck, A. J. R., and Altelaar, M. (2023) Elucidating fibroblast growth factor-induced kinome dynamics using targeted mass spectrometry and dynamic modeling. *Mol. Cell. Proteomics.* **22**, 100594
26. Duke, G. M., and Palmenberg, A. C. (1989) Cloning and synthesis of infectious cardiovirus RNAs containing short, discrete poly(C) tracts. *J. Virol.* **63**, 1822–1826
27. Hato, S. V., Ricour, C., Schulte, B. M., Lanke, K. H. W., de Bruijni, M., Zoll, J., *et al*. (2007) The mengovirus leader protein blocks interferon-α/β gene transcription and inhibits activation of interferon regulatory factor 3: mengovirus L blocks IFN transcription and IRF-3 activation. *Cell. Microbiol.* **9**, 2921–2930
28. Lanke, K. H. W., van der Schaar, H. M., Belov, G. A., Feng, Q., Duijsings, D., Jackson, C. L., *et al*. (2009) GBF1, a guanine nucleotide exchange factor for Arf, is Crucial for coxsackievirus B3 RNA replication. *J. Virol.* **83**, 11940–11949
29. Maciejewski, S., Ullmer, W., and Semler, B. L. (2018) VPg unlinkase/TDP2 in cardiovirus infected cells: Re-localization and proteolytic cleavage. *Virology* **516**, 139–146
30. Post, H., Penning, R., Fitzpatrick, M. A., Garrigues, L. B., Wu, W., MacGillavry, H. D., *et al*. (2017) Robust, sensitive, and automated phosphopeptide enrichment optimized for low sample amounts applied to primary hippocampal neurons. *J. Proteome Res.* **16**, 728–737
31. Pino, L. K., Searle, B. C., Bollinger, J. G., Nunn, B., MacLean, B., and MacCoss, M. J. (2020) The Skyline ecosystem: informatics for quantitative mass spectrometry proteomics. *Mass. Spectrom. Rev.* **39**, 229–244
32. Escher, C., Reiter, L., MacLean, B., Ossola, R., Herzog, F., Chilton, J., *et al*. (2012) Using iRT, a normalized retention time for more targeted measurement of peptides. *Proteomics* **12**, 1111–1121
33. Schweiger, R., and Linial, M. (2010) Cooperativity within proximal phosphorylation sites is revealed from large-scale proteomics data. *Biol. Direct.* **5**, 6
34. Villén, J., Beausoleil, S. A., Gerber, S. A., and Gygi, S. P. (2007) Large-scale phosphorylation analysis of mouse liver. *Proc. Natl. Acad. Sci. U. S. A.* **104**, 1488–1493
35. Courcelles, M., Bridon, G., Lemieux, S., and Thibault, P. (2012) Occurrence and detection of phosphopeptide isomers in large-scale phosphoproteomics experiments. *J. Proteome Res.* **11**, 3753–3765
36. Locard-Paulet, M., Bouyssié, D., Froment, C., Burlet-Schiltz, O., and Jensen, L. J. (2020) Comparing 22 popular phosphoproteomics pipelines for peptide identification and site localization. *J. Proteome Res.* **19**, 1338–1345
37. Peyssonnaux, C., and Eychène, A. (2001) The Raf/MEK/ERK pathway: new concepts of activation. *Biol. Cell* **93**, 53–62
38. Tibbles, L. A., and Woodgett, J. R. (1999) The stress-activated protein kinase pathways. *Cell. Mol. Life Sci.* **55**, 1230–1254
39. Dai, Q., Zhang, D., Yu, H., Xie, W., Xin, R., Wang, L., *et al*. (2017) Berberine restricts coxsackievirus B type 3 replication via inhibition of c-Jun N-terminal kinase (JNK) and p38 MAPK activation in vitro. *Med. Sci. Monit.* **23**, 1448–1455
40. Iordanov, M. S., Paranjape, J. M., Zhou, A., Wong, J., Williams, B. R. G., Meurs, E. F., *et al*. (2000) Activation of p38 mitogen-activated protein kinase and c-Jun NH_2 -terminal kinase by double-stranded RNA and encephalomyocarditis virus: involvement of RNase L, protein kinase R, and alternative pathways. *Mol. Cell. Biol.* **20**, 617–627
41. Si, X., Luo, H., Morgan, A., Zhang, J., Wong, J., Yuan, J., *et al*. (2005) Stress-activated protein kinases are involved in coxsackievirus B3 viral progeny release. *J. Virol.* **79**, 13875–13881
42. Lizcano-Perret, B., Lardinois, C., Wavreil, F., Hauchamps, P., Herinckx, G., Sorgeloos, F., *et al*. (2022) Cardiovirus leader proteins retarget RSK kinases toward alternative substrates to perturb nucleocytoplasmic traffic. *PLOS Pathog.* **18**, e1011042
43. Porter, F. W., Brown, B., and Palmenberg, A. C. (2010) Nucleoporin phosphorylation triggered by the encephalomyocarditis virus leader protein is mediated by mitogen-activated protein kinases. *J. Virol.* **84**, 12538–12548
44. Romeo, Y., Zhang, X., and Roux, P. P. (2012) Regulation and function of the RSK family of protein kinases. *Biochem. J.* **441**, 553–569
45. Cai, Z., Chehab, N. H., and Pavletich, N. P. (2009) Structure and activation mechanism of the CHK2 DNA damage checkpoint kinase. *Mol. Cell* **35**, 818–829
46. Turnell, A. S., and Grand, R. J. (2012) DNA viruses and the cellular DNA-damage response. *J. Gen. Virol.* **93**, 2076–2097
47. Zannini, L., Delia, D., and Buscemi, G. (2014) CHK2 kinase in the DNA damage response and beyond. *J. Mol. Cell Biol.* **6**, 442–457
48. Sarkar, R., Patra, U., Lo, M., Mukherjee, A., Biswas, A., and Chawla-Sarkar, M. (2020) Rotavirus activates a noncanonical ATM-Chk2 branch of DNA damage response during infection to positively regulate viroplasm dynamics. *Cell. Microbiol.* **22**, e13149
49. Kuo, L. J., and Yang, L.-X. (2008) γ-H2AX – a novel biomarker for DNA double-strand breaks. *In Vivo* **22**, 305–309
50. Malumbres, M. (2014) Cyclin-dependent kinases. *Genome Biol.* **15**, 122
51. Aranda, S., Laguna, A., and de la Luna, S. (2011) DYRK family of protein kinases: evolutionary relationships, biochemical properties, and functional roles. *FASEB J.* **25**, 449–462
52. Kim, Y. H., Choi, C. Y., Lee, S.-J., Conti, M. A., and Kim, Y. (1998) Homeodomain-interacting protein kinases, a novel family of Co-repressors for homeodomain transcription factors. *J. Biol. Chem.* **273**, 25875–25879
53. Parsons, S. J., and Parsons, J. T. (2004) Src family kinases, key regulators of signal transduction. *Oncogene* **23**, 7906–7909
54. Puca, R., Nardinocchi, L., Givol, D., and D'Orazi, G. (2010) Regulation of p53 activity by HIPK2: molecular mechanisms and therapeutical implications in human cancer cells. *Oncogene* **29**, 4378–4387
55. Van den Broeke, C., Radu, M., Chernoff, J., and Favoreel, H. W. (2010) An emerging role for p21-activated kinases (Paks) in viral infections. *Trends Cell Biol.* **20**, 160–169
56. Bacon, C. W., and D'Orso, I. (2019) CDK9: a signaling hub for transcriptional control. *Transcription* **10**, 57–75
57. Hu, D., Mayeda, A., Trembley, J. H., Lahti, J. M., and Kidd, V. J. (2003) CDK11 complexes promote pre-mRNA splicing. *J. Biol. Chem.* **278**, 8623–8629
58. Zhang, H., Zeng, L., Liu, Q., Jin, G., Zhang, J., Li, Z., *et al*. (2021) CVB3 VP1 interacts with MAT1 to inhibit cell proliferation by interfering with Cdk-activating kinase complex activity in CVB3-induced acute pancreatitis. *PLOS Pathog.* **17**, e1008992
59. Aloise, C., Schipper, J. G., de Groot, R. J., and van Kuppeveld, F. J. (2022) Move and countermove: the integrated stress response in picorna- and coronavirus-infected cells. *Curr. Opin. Immunol.* **79**, 102254
60. Belov, G. A., and Sztul, E. (2014) Rewiring of cellular membrane homeostasis by picornaviruses. *J. Virol.* **88**, 9478–9489
61. Feng, Q., Langereis, M. A., and van Kuppeveld, F. J. M. (2014) Induction and suppression of innate antiviral responses by picornaviruses. *Cytokine Growth Factor Rev.* **25**, 577–585
62. Flather, D., and Semler, B. L. (2015) Picornaviruses and nuclear functions: targeting a cellular compartment distinct from the replication site of a positive-strand RNA virus. *Front. Microbiol.* **6**, 594
63. Dorobantu, C. M., Albulescu, L., Harak, C., Feng, Q., van Kampen, M., Strating, J. R. P. M., *et al*. (2015) Modulation of the host lipid landscape to promote RNA virus replication: the picornavirus encephalomyocarditis virus converges on the pathway used by hepatitis C virus. *PLOS Pathog.* **11**, e1005185
64. Hsu, N.-Y., Ilnytska, O., Belov, G., Santiana, M., Chen, Y.-H., Takvorian, P. M., *et al*. (2010) Viral reorganization of the secretory pathway generates distinct organelles for RNA replication. *Cell* **141**, 799–811
65. Sorgeloos, F., Peeters, M., Hayashi, Y., Borghese, F., Capelli, N., Drappier, M., *et al*. (2022) A case of convergent evolution: several viral and bacterial pathogens hijack RSK kinases through a common linear motif. *Proc. Natl. Acad. Sci. U. S. A.* **119**, e2114647119
66. Lai, Y., Wang, M., Cheng, A., Mao, S., Ou, X., Yang, Q., *et al*. (2020) Regulation of apoptosis by enteroviruses. *Front. Microbiol.* **11**, 1145
67. Shi, W., Hou, X., Li, X., Peng, H., Shi, M., Jiang, Q., *et al*. (2013) Differential gene expressions of the MAPK signaling pathway in enterovirus 71-infected rhabdomyosarcoma cells. *Braz. J. Infect. Dis.* **17**, 410–417
68. Zhang, B., Chen, X., Yue, H., Ruan, W., Qin, S., and Tang, C. (2018) Transcriptomic analysis reveals that enterovirus F strain SWUN-AB001 infection activates JNK/SAPK and p38 MAPK signaling pathways in MDBK cells. *BMC Vet. Res.* **14**, 395

69. Su, Y., Wu, T., Yu, X.-Y., Huo, W.-B., Wang, S.-H., Huan, C., *et al*. (2022) Inhibitory effect of tanshinone IIA, resveratrol and silibinin on enterovirus 68 production through inhibiting ATM and DNA-PK pathway. *Phytomedicine* **99**, 153977
70. Hammack, C., Ogden, S. C., Madden, J. C., Medina, A., Xu, C., Phillips, E., *et al*. (2019) Zika virus infection induces DNA damage response in human neural progenitors that enhances viral replication. *J. Virol.* **93**, e00638-19
71. Lopez, A., Nichols Doyle, R., Sandoval, C., Nisson, K., Yang, V., and Fregoso, O. I. (2022) Viral modulation of the DNA damage response and innate immunity: two sides of the same coin. *J. Mol. Biol.* **434**, 167327
72. Luftig, M. A. (2014) Viruses and the DNA damage response: activation and antagonism. *Annu. Rev. Virol.* **1**, 605–625
73. Mekawy, A. S., Alaswad, Z., Ibrahim, A. A., Mohamed, A. A., AlOkda, A., and Elserafy, M. (2022) The consequences of viral infection on host DNA damage response: a focus on SARS-CoVs. *J. Genet. Eng. Biotechnol.* **20**, 104
74. Nikitin, P. A., and Luftig, M. A. (2012) The DNA damage response in viral-induced cellular transformation. *Br. J. Cancer* **106**, 429–435
75. Ryan, E., Hollingworth, R., and Grand, R. (2016) Activation of the DNA damage response by RNA viruses. *Biomolecules* **6**, 2
76. Feuer, R., Mena, I., Pagarigan, R., Slifka, M. K., and Whitton, J. L. (2002) Cell cycle status affects coxsackievirus replication, persistence, and reactivation in vitro. *J. Virol.* **76**, 4430–4440
77. Luo, H., Zhang, J., Dastvan, F., Yanagawa, B., Reidy, M. A., Zhang, H. M., *et al*. (2003) Ubiquitin-dependent proteolysis of cyclin D1 is associated with coxsackievirus-induced cell growth arrest. *J. Virol.* **77**, 1–9
78. Mallucci, L., Wells, V., and Beare, D. (1985) Cell cycle position and expression of encephalomyocarditis virus in mouse embryo fibroblasts. *J. Gen. Virol.* **66**, 1501–1506
79. Wang, Z., Zhong, T., Wang, Y., Song, F., Yu, X., Xing, L., *et al*. (2017) Human enterovirus 68 interferes with the host cell cycle to facilitate viral production. *Front. Cell. Infect. Microbiol.* **7**, 29
80. Yu, J., Zhang, L., Ren, P., Zhong, T., Li, Z., Wang, Z., *et al*. (2015) Enterovirus 71 mediates cell cycle arrest in S phase through non-structural protein 3D. *Cell Cycle* **14**, 425–436
81. Krajewska, M., Dries, R., Grassetti, A. V., Dust, S., Gao, Y., Huang, H., *et al*. (2019) CDK12 loss in cancer cells affects DNA damage response genes through premature cleavage and polyadenylation. *Nat. Commun.* **10**, 1757
82. Magnuson, B., Bedi, K., Narayanan, I. V., Bartkowiak, B., Blinkiewicz, H., Paulsen, M. T., *et al*. (2022) CDK12 regulates co-transcriptional splicing and RNA turnover in human cells. *iScience* **25**, 105030
83. Anshabo, A. T., Milne, R., Wang, S., and Albrecht, H. (2021) CDK9: a comprehensive review of its biology, and its role as a potential target for anti-cancer agents. *Front. Oncol.* **11**, 678559
84. Gajdušková, P., Ruiz de los Mozos, I., Rájecký, M., Hluchý, M., Ule, J., and Blazek, D. (2020) CDK11 is required for transcription of replication-dependent histone genes. *Nat. Struct. Mol. Biol.* **27**, 500–510
85. Aminev, A. G., Amineva, S. P., and Palmenberg, A. C. (2003) Encephalomyocarditis virus (EMCV) proteins 2A and 3BCD localize to nuclei and inhibit cellular mRNA transcription but not rRNA transcription. *Virus Res.* **95**, 59–73
86. Sharma, R., Raychaudhuri, S., and Dasgupta, A. (2004) Nuclear entry of poliovirus protease-polymerase precursor 3CD: implications for host cell transcription shut-off. *Virology* **320**, 195–205
87. Raudvere, U., Kolberg, L., Kuzmin, I., Arak, T., Adler, P., Peterson, H., *et al*. (2019) g:Profiler: a web server for functional enrichment analysis and conversions of gene lists (2019 update). *Nucleic Acids Res.* **47**, W191–W198